Journal of Molecular Catalysis A: Chemical 406 (2015) 97–105

Contents lists available at ScienceDirect

Journal of Molecular Catalysis A: Chemical

journal homepage: www.elsevier.com/locate/molcata

Editor's choice paper

Synthesis of Fe_3O_4@SiO_2@ZnO–Ag core–shell microspheres for the repeated photocatalytic degradation of rhodamine B under UV irradiation

Jian Wang[a,b], Jinghai Yang[c,*], Xiuyan Li[c,*], Bing Wei[c], Dandan Wang[a,b], Hang Song[a], Hongju Zhai[c], Xuefei Li[c]

[a] Changchun Institute of Optics, Fine Mechanics and Physics, Chinese Academy of Sciences, Changchun 130033, PR China
[b] University of Chinese Academy of Sciences, Beijing 100049, PR China
[c] Key Laboratory of Functional Materials Physics and Chemistry of the Ministry of Education, Jilin Normal University, Siping 136000, PR China

ARTICLE INFO

Article history:
Received 5 April 2015
Received in revised form 25 May 2015
Accepted 28 May 2015
Available online 30 May 2015

Keywords:
Core–shell structure
ZnO
Magnetic separation
Photocatalytic activity

ABSTRACT

Herein, novel Fe_3O_4@SiO_2@ZnO–Ag core–shell microstructures were synthesized through template synthesis and layer-by-layer deposition. The obtained samples were characterized in terms of morphology, composition, optical and magnetic property by various analytical techniques and subsequently tested for the photocatalytic activities. In comparison with Fe_3O_4@SiO_2@ZnO, the as-obtained multi-shelled Fe_3O_4@SiO_2@ZnO–Ag hierarchical microspheres exhibit a significant enhanced photocatalytic activity toward the photodegradation of Rhodamine B (RhB) aqueous solution under UV light. The enhanced photocatalytic activities of the core–shell photocatalyst are primarily ascribed to the reduced recombination probability of photogenerated electrons/holes in the surface of hierarchical microspheres. Moreover, the hierarchical microstructured Fe_3O_4@SiO_2@ZnO–Ag photocatalysts could be easily collected and separated by using a magnetic field and reused without any appreciable decrease on photocatalytic efficiency after running six times. The enhanced photocatalytic performance and magnetic recyclability, in combination with the superior chemical stability, make these multifunctional microstructures promising candidates to eliminate aquatic contaminants and meet the demands of future environmental issues.

1. Introduction

Along with worsening of water pollution, organic pollutants are becoming one of the most major sources because of their huge volume of production from industry, slow toxicity, and weak self-degradation [1]. A variety of conventional methods in different fields of science have been applied to carrying out water purification, including chemical oxidation, membrane processes, liquid extraction, filtration and coagulation/flocculation/sedimentation, biological treatment, and so on, which are proved to be low efficiency and expansive for the treatment of these pollutants [1,2]. Semiconductor photocatalysis, as a "green chemistry" technology, has been recognized as an ideal and effective candidate in contaminants degradation due to its efficient degradation rate, high mineralization efficiency and low toxigenicity, ideally producing CO_2 and H_2O as the final products [3,4].

Since the first report about semiconductor photocatalysis by Fujishima and Honda in 1972 [5], several semiconductors have been utilized for photocatalytic degradation of organic pollutants [6–11]. Among them, zinc oxide (ZnO) with band gap energy (3.37 eV at room temperature) has attracted extensive attention for its photocatalytic applications owing to its high photosensitivity, high quantum efficiency, thermal stability, low cost, and nontoxic [12–14]. Because the photocatalytic redox reaction mainly takes place on the surface of the photocatalysts, ZnO micro/nanoparticles which have large solid to liquid contact areas were always used as photocatalysts [10,13,15].

For practical photocatalytic applications in aqueous environments, easy separation and recycling is very important. Failing to recycle these nanostructures not only increases the cost, but also possibly brings secondary pollution. However, the separation of those fine photocatalysts requires usually complex and inefficient centrifugation or filtration processes, which in turn lead to huge

* Corresponding authors. Tel.: +86 434 3294566; fax: +86 434 3294566.
E-mail addresses: jhyang1@jlnu.edu.cn (J. Yang), lixiuyan@126.com (X. Li).

http://dx.doi.org/10.1016/j.molcata.2015.05.023
1381-1169/

increase in the practical running costs. To address this problem, many researchers have tried to immobilize the photocatalysts on supporting materials such as organic fiber or zeolite, which can conspicuously improve the separation efficiency [16–18]. However, owing to the significant decrease of the solid to liquid contact areas caused by fixation these immobilized photocatalysts always have weaker photocatalytic performance compared with that of the corresponding micro/nanoparticles suspensions [19]. An effective solution to this issue is the incorporation of magnetic components by virtue of the unique superiority of the magnetic particles in removing and recycling [20,21]. Therefore, lots of researches have been concentrated on the incorporation of magnetic components into ZnO micro/nanoparticles based photocatalysts, which can be reused efficiently from the aqueous environment by simply applying appropriate magnetic fields [22,23]. Because of instability of magnetite particles under harsh environments, especially in acidic conditions, it is often need to coat them with an inert silica layer, which can also inhibit the transfer of electrons–holes from photocatalysis active area to core particle and avoid the reduction of photocatalytic activity [23–25]. For this purpose, coating a silica shell is necessary.

To enhance the photocatalytic activity of semiconductor photocatalyst farther, many researches have been deposited noble metals in the semiconductor. The depositing of noble metal (such as Pt, Ag, and Au) can change electron distribution in the above system and affect the surface properties of the semiconductor photocatalyst, thereby improving the photocatalytic performance [26–29]. In addition, the selection of an appropriate noble metal which is much cheaper and more efficient is an important issue also. Moonsiri et al. have compared the photoctalytic activity of depositing Pt and Ag on TiO_2, and the results revealed that the photocatalytic performance of TiO_2–Ag was better than that of TiO_2–Pt owing to the ability of Ag to produce more superoxide radicals and to the increased rate of direct hole oxidation [30]. Base on the lower cost and excellent ability in enhancing the catalytic activity of semiconductor photocatalyst, more and more researches were carried to study the effect of Ag depositing in photocatalytic reaction [31–33].

Although a great deal of effort has been spent to solve the above concerns, including stable recyclability, enhancement of active sites in surface, and efficient electron–hole separation properties, few researches have taken into account all these terms simultaneously and settled them effectively. In addition, it remains a great challenge to address these issues together and integrate multiple functional components into one uniform unit at the microscale to maximize the photocatalytic efficiency. Herein, we develop a simple and novel route to prepare Fe_3O_4@SiO_2@ZnO–Ag core–shell microspheres. The final Fe_3O_4@SiO_2@ZnO–Ag core–shell microspheres exhibit excellent photocatalytic decomposition activity towards Rhodamine B (RhB) under UV light irradiation and superior recyclability.

2. Experiments

2.1. Materials and reagents

Ferric chloride hexahydrate ($FeCl_3 \times 6H_2O$), ethylene glycol (EG), sodium acetate (NaAc), lauryl sodium sulfate (SDS), dimethylformamide (DMF), Zinc nitrate hexahydrate ($ZnNO_3 \times 6H_2O$), sodium hydroxide (NaOH), ethylalcohol (C_2H_5OH), tetraethyl orthosilicate (TEOS), silver nitrate ($AgNO_3$), Polyvinylpyrrolidone (PVP), concentrated ammonia solution (25 wt%) are of analytical grade and purchased from Sinopharm Chemical Reagent Co., Ltd. All the chemicals used in this experiment were of analytical grade and were used without further purification. Deionized water (resistivity > 18.0 MΩ cm) was used throughout the experiment.

2.2. Synthesis of Fe_3O_4 microspheres

By using a modified solvothermal reaction, Fe_3O_4 magnetic spheres were prepared according to a former research [34]. In a typical synthesis, $FeCl_3 \times 6H_2O$ (2.16 g) was dissolved in EG (80 mL) and stirred for 1 h to form a clear yellow solution. NaAc (3.6 g) and SDS (0.5 g) were then added to this solution and further vigorously stirred for 1 h. Subsequently, the resulting mixture solution was sealed in a teflonlined stainless-steel autoclave (100 mL capacity) and maintained at 200 °C for 12 h, and allowed to cool to room temperature. The obtained black products were washed several times with ethanol and deionized water and then dried under vacuum at 60 °C for 6 h.

2.3. Synthesis of Fe_3O_4@SiO_2 microspheres

Fe_3O_4@SiO_2 microspheres could be fabricated by a Stöber method with some modification [35]. Briefly, Fe_3O_4 (0.3 g) microspheres were added into a mixture solution containing absolute ethanol (150.0 mL), deionized water (50.0 mL), and concentrated ammonia solution (3.4 mL, 25 wt%) under sonication and stirred for 0.5 h. TEOS (0.5 mL) was then added in sequence to the suspension described above. Finally, after mechanical stirred at room temperature for 4 h, the Fe_3O_4@SiO_2 microspheres were separated, washed with ethanol and then dried at 60 °C for 6 h in vacuum.

2.4. Synthesis of Fe_3O_4@SiO_2@ZnO microspheres

Fe_3O_4@SiO_2@ZnO microspheres could be fabricated by a simple coprecipitation method. The typical synthesis process was as follows: $ZnNO_3 \times 6H_2O$ (0.3 g) was dissolved in DMF (50 mL), forming a 0.02 M solution, NaOH (0.04 g) was dissolved in deionized water (2 mL), forming a 0.5 M solution. Fe_3O_4@SiO_2 (about 0.24 g), were uniformly dispersed in DMF (50 mL) by ultrasonication, and then the $ZnNO_3 \times 6H_2O$ solution was added slowly to the DMF (50 mL) while being ultrasonicated. After ultrasonicating for about 30 min, NaOH solution was added slowly to the solution. After continuous ultrasonication for 1 h, the mixed solution was aged at room temperature for 1 day. The precipitate was filtered, washed with ethanol and deionized water, and dried dried at 60 °C for 6 h. The as-prepared precursor was loaded into a quartz boat and put in a hot zone of a furnace. After calcination at 500 °C for 2 h in Ar atmosphere, the product was cooled to room temperature, and Fe_3O_4@SiO_2@ZnO microspheres were finally obtained.

2.5. Synthesis of Fe_3O_4@SiO_2@ZnO-Ag microspheres

Fe_3O_4@SiO_2@ZnO–Ag microspheres were synthesized through a simple in situ wet chemistry method according to a previously published work with some modification [36]. First, Fe_3O_4@SiO_2@ZnO microstructures (0.12 g) were dispersed into Tollens' reagent (30 mL, 5×10^{-3} M), mechanical stir at room temperature. After 30 min mechanical stir, the $[Ag(NH_3)_2]^+$ ions can be adsorbed by the surfaces of Fe_3O_4@SiO_2@ZnO microstructures., Then PVP (0.2 g) dispersed in ethanol (30 mL) was added into the former mixture. The reaction solution was maintaining at 70 °C for 4 h with a reflux apparatus. The products were washed with ethanol and deionized water for three times, and dried at 60 °C for 10 h.

2.6. Characterization

Morphologies of all samples were characterized by a field emission scanning electron microscope (FESEM, JEOL 7800F). Transmission electron microscopy (TEM), high-resolution TEM (HRTEM) and element mapping imaging were performed by a FEI Tenai G^2 F20 microscope. The as-prepared samples were dispersed

in ethanol and then dropped onto a carbon film supported on a copper grid. The structure and composition of the products were studied with a D/max-2500 copper rotating-anode X-ray powder diffraction (XRD) with Cu K α radiation of wavelength λ = 1.5406 Å (40 kV, 200 mA). X-ray photoelectron spectroscopy (XPS) analysis was accomplished using a Thermo Scientific ESCALAB 250Xi A1440 system. The room temperature photoluminescence (PL) analysis was performed using a Renishaw inVia micro-PL spectrometer (325 nm, He-Cd laser). The magnetic behavior was analyzed using a vibrating sample magnetometer (VSM) on a physical property measurement system (Lake Shore 7407) with the applied field from −14500 to 14500 Oe.

2.7. Photocatalytic degradation of Rhodamine B (RhB)

The photocatalytic performances of the prepared catalysts were evaluated by the photocatalytic decomposition of Rhodamine B (RhB) aqueous solution. In the experiment, 60 mg of the photocatalyst was dispersed in 60 mL of RhB solution (7 mg/L). A 250 W high-pressure mercury lamp (central emission wavelength at 365 nm) was used to irradiate the solution. The average light energy density was estimated to be 22.11 mW × cm^{-2}. Before illumination, the suspension was mechanically stirred in dark for 15 min to ensure an adsorption–desorption equilibrium between the photocatalyst and RhB. The reaction solutions were sampled at 15 min illumination intervals, and the corresponding UV–vis spectra (measured in the range of 350–750 nm) were recorded to monitor the progress of the degradation of RhB by an UV–vis spectrophotometer (UV-5800PC, Shanghai Metash Instruments Co., Ltd.). When each photocatalytic experiment ended, the catalyst was separated from the solution by a magnet. The recycled magnetic catalyst was then washed with ethanol and deionized water for several times. After that, the obtained magnetic microspheres were redispersed in 60 mL of RhB solution (7 mg/L), and the new photocatalytic cycle began. The photodegradation efficiency (%) of RhB was calculated from the following expression: the RhB photodegradation efficiency (%) = $(C_0 - C_t)/C_0 \times 100\%$, where C_0 and C_t represent the initial concentration and the concentration after different UV irradiation time intervals, respectively.

3. Results and discussion

3.1. Morphology and structure of the as-prepared microspheres

Fe_3O_4@SiO_2@ZnO–Ag microspheres were designed strategically and fabricated by layer-by-layer deposition. The left image in Fig. 1 shows the preparation schematic outline of the multilayer core/shell structures. In the first step, solvothermal method is employed to obtain Fe_3O_4 microspheres. As revealed in Figs. 1 a and 2 a , the diameter of obtained Fe_3O_4 microspheres is about 300 nm.

Subsequently, a silica shell was coated via hydrolysis of TEOS in accordance with the classical Stöber approach [35]. The coating of SiO_2 shell can prevent Fe_3O_4 particles from photocorrosion and chemical etching. This inert shell can also interdict the charge transfer between the Fe_3O_4 core and the catalyst shell which has negative effect on the photocatalytic activity [28,36]. From the FESEM image shown in Fig. 1b we can see the morphological properties of Fe_3O_4@SiO_2 microspheres are similar to that of pure Fe_3O_4. Particle size Fe_3O_4@SiO_2 microspheres is about 350 nm. As shown in Fig. 2b, the Fe_3O_4@SiO_2 microspheres have an obviously core–shell structure. The Fe_3O_4 microspheres were coated with silica layer with a thickness of about 25 nm.

After a further coating process, Fe_3O_4@SiO_2@ZnO microspheres were formed via a simple coprecipitation method and then calcined at 500 °C in Ar atmosphere for 2 h to obtain highly crystalline ZnO. According to SEM images, the morphology of the products transforms from the spherical shape with a smooth surface (Fig. 1b) to a rough surface (Fig. 1c). The detailed morphology of these burr-shaped hierarchical architectures is revealed by the TEM image in Fig. 2c, which clearly displays a typical core–shell structure composed of a Fe_3O_4 core, middle SiO_2 layer and a rough ZnO shell with a thickness of about 5 nm.

Finally, an in situ wet chemistry method was chosen to obtain Fe_3O_4@SiO_2@ZnO–Ag core–shell structured microspheres, which consumes less time and has other advantages such as high yield, mild reaction condition and simple operation. As shown in SEM image (Fig. 1d) the size of those microspheres are uniform. The TEM images (Fig. 2d and e) support that a lot of small Ag nanoparticles are well dispersed on the surface of Fe_3O_4@SiO_2@ZnO microspheres. There are two different lattice fringes appeared in HRTEM image (Fig. 2f). The fringe distance appeared in the left part of Fig. 2f is 0.235 nm, which is close to the lattice fringes of (1 1 1) plane of Ag (JCPDS card No. 04-0783). Another fringe distance appeared in the right part of Fig. 2f is about 0.257 nm, which corresponds to the (0 0 2) plane of hexagonal crystal structure of ZnO (JCPDS card No. 36-1451). As a result, it means Ag–ZnO heterostructure formed on the surface of core–shell microspheres.

To further confirm the formation of Fe_3O_4@SiO_2@ZnO–Ag composite, samples were analyzed by electron mapping image analysis (Fig. 3). The distribution map of elements Fe, Si, Zn and Ag is displayed in Fig. 3b–f with different color, respectively. It indicates the presence of SiO_2, ZnO and Ag in the outer surface of Fe_3O_4 microspheres. The images also show that SiO_2, ZnO and Ag nanoparticles are well-dispersed on the surface of Fe_3O_4 microspheres. In conclusion, high-density ZnO and Ag NPs have been immobilized on the surface of core-shell microspheres.

The composition and crystallinity of the as-prepared samples were investigated with XRD technology. As shown in Fig. 4, all of the identified peaks in the XRD pattern (Fig. 4a) can be readily indexed to magnetite Fe_3O_4, based on the standard data for magnetite (JCPDS No. 19-0629). No impurity was observed. There are six major diffraction peaks at 30.08°, 35.40°, 43.02°, 53.38°, 56.86°, and 62.46° observed for the Fe_3O_4 microspheres, which can be assigned to (2 2 0), (3 1 1), (4 0 0), (4 2 2), (5 1 1), and (4 4 0) planes of the face-centered cubic structure of magnetite (JCPDS No. 19-0629), respectively. The coating of amorphous SiO_2 layer did not change the structure of Fe_3O_4. In the case of Fe_3O_4@SiO_2@ZnO composites, the peaks of face-centered cubic structured magnetite were observed in the composites, revealing that the Fe_3O_4 nanocrystals do not change their phases. The added major diffraction peaks at 31.96°, 34.64°, 36.46°, 47.72°, and 56.76° (Fig. 1b) can be readily indexed to the hexagonal ZnO structure according to the standard JCPDS (No. 36-1451). Compared with Fig. 4a–c besides the characteristic diffraction of Fe_3O_4 and ZnO, the obvious diffraction peaks at 38.11°, 44.30°, 64.41°, and 77.49° could be indexed to cubic phase silver (JCPDS No. 04-0783), revealing that Ag nanoparticles have been loaded on the surface of core–shell microspheres.

3.2. Surface structure of the as-prepared microspheres

To clarify the elemental and chemical states of the prepared core–shell microspheres, the Fe_3O_4@SiO_2@ZnO–Ag was studied by XPS analysis and compared with that of Fe_3O_4@SiO_2@ZnO. Fig. 5a shows the survey XPS spectra from 0 to 1200 eV of the samples. The peaks on the curve of Fe_3O_4@SiO_2@ZnO–Ag microcomposite are assigned to Si, Zn, O, Ag, and C elements. The C peak (C 1s = 284.8 eV) is assigned to the adventitious carbonbased contaminant. Therefore, it is means that Si, Zn, O, and Ag exist in Fe_3O_4@SiO_2@ZnO–Ag microcomposite, while Si, Zn, and O exist in Fe_3O_4@SiO_2@ZnO microspheres. Fe was not observed in two survey XPS spectra. That is because XPS spectra is a highly surface-specific

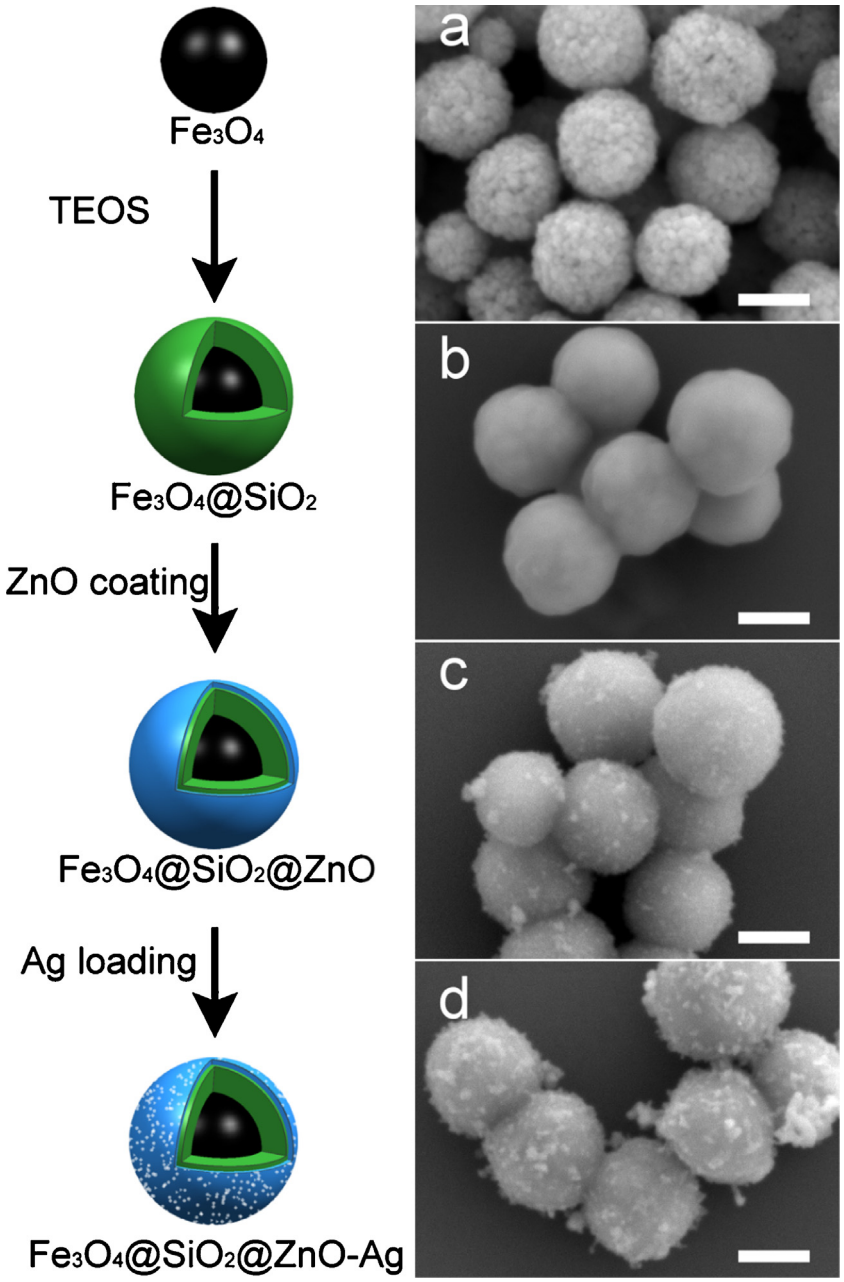

Fig. 1. Left: Schematic illustration of the fabrication process of Fe_3O_4@SiO_2@ZnO–Ag microspheres; Right: FESEM images of the as-prepared products: (a) Fe_3O_4, (b) Fe_3O_4@SiO_2, (c) Fe_3O_4@SiO_2@ZnO, (d) Fe_3O_4@SiO_2@ZnO–Ag. (All scale bars are 200 nm).

technique and it can only reach ~10 nm depth of the sample [36]. Fe_3O_4@SiO_2@ZnO–Ag core–shell microsphere synthesized in our work has a 25 nm SiO_2 layer, and there is additional ZnO layer and Ag particles loading upon the ZnO. As a result the inner Fe_3O_4 core was too far away from the particle surface. So the missing of signal binding energy of Fe 2p in the XPS spectra is reasonable. The high resolution XPS spectra of the Zn 2p are analyzed in Fig. 5b. Two peaks in the curves of the two samples at 1020.7 and 1043.8 eV can be indexed to Zn $2p_{3/2}$ and Zn $2p_{1/2}$, respectively. It confirms that Zn element exists mainly in the form of Zn^{2+} chemical state on the sample surfaces. Furthermore, because XPS is a highly surface-specific technique with a typical analysis depth of about 10 nm, the intensity of Zn 2p signal is decreased after the loading of Ag nanoparticles on the surface of ZnO. Fig. 5c presents the XPS spectra of the Ag 3d peak from the samples of Fe_3O_4@SiO_2@ZnO–Ag. Two peaks in the curves of the two samples at 366.7 and 372.7 eV can be indexed to Ag $3d_{5/2}$ and Ag $3d_{3/2}$ of Ag0, respectively. It means that the Fe_3O_4@SiO_2@ZnO–Ag core–shell microspheres contained Ag NPs. Moreover, it is shown that the binding energy (BE) of Ag $3d_{5/2}$ for Fe_3O_4@SiO_2@ZnO–Ag shifts remarkably to a lower binding energy compared with that of the pure Ag nanoparticles and the bulk Ag0 (the standard binding energy of Ag $3d_{5/2}$ for bulk Ag0 is about 368.2 eV). This suggests that the electron density of Ag is decreased. Once the Ag NPs are loaded on the surface of ZnO, electron transfer occurs from Ag to the conduction band (CB) of ZnO because the work function of Ag is smaller than that of ZnO [37,38]. This XPS result could reveal the interaction between Ag and ZnO.

3.3. Optical property of the as-prepared microspheres

The photoluminescence spectra (PL) of the prepared Fe_3O_4@SiO_2@ZnO and Fe_3O_4@SiO_2@ZnO–Ag core–shell micro-

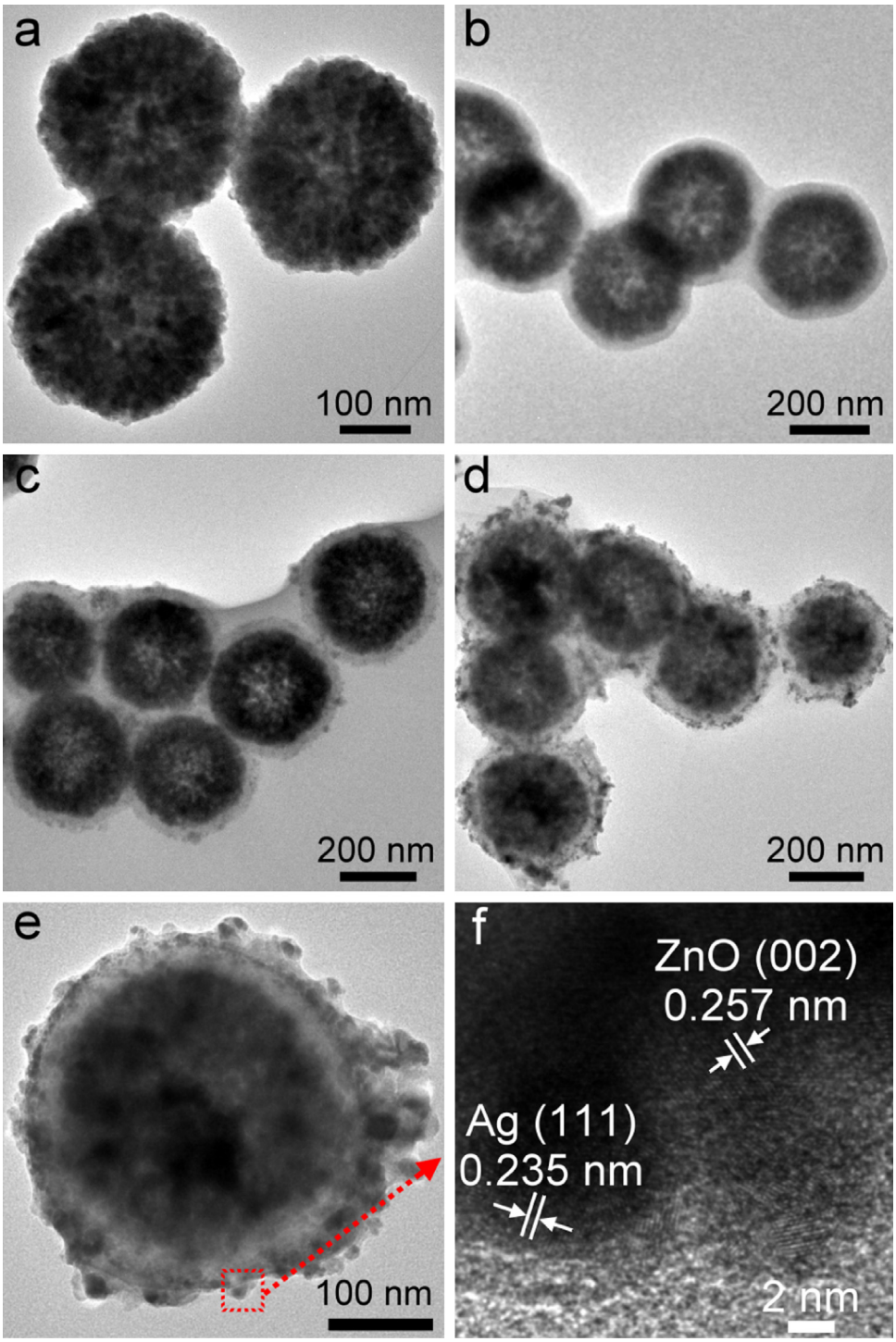

Fig. 2. TEM images of the as-prepared products: (a) Fe_3O_4, (b) Fe_3O_4@SiO_2, (c) Fe_3O_4@SiO_2@ZnO, (d) and (e) Fe_3O_4@SiO_2@ZnO–Ag. (f) HRTEM image for the select area in (e).

composite (λ_{ex} = 325 nm) are shown in Fig. 6. It can be employed to determine the charge recombination and migration efficiency of the ZnO and Ag–ZnO. The bule emission intensity of the PL spectrum of Fe_3O_4@SiO_2@ZnO–Ag was lower than that of Fe_3O_4@SiO_2@ZnO, suggesting that the loading of Ag NPs could quench the fluorescence from the ZnO nanoparticles and prolong electron–hole pair lifetime [31,39]. A lower photoluminescence intensity means a lower electron–hole recombination rate, and hence a longer lifetime of the photogenerated carriers [31,39]. In general, the efficient charge separation and inhibited electron–hole recombination by Ag NPs are favorable for enhancing the photocatalytic activity of Fe_3O_4@SiO_2@ZnO. The PL spectra show that loading Ag NPs to the surface of ZnO could effectively inhibit electron–hole recombination during the photocatalytic reaction under UV light irradiation.

3.4. Photocatalytic property of the as-prepared microspheres

To test the photocatalytic performance of the core–shell microspheres, the degradation of RhB was chosen as a model reaction

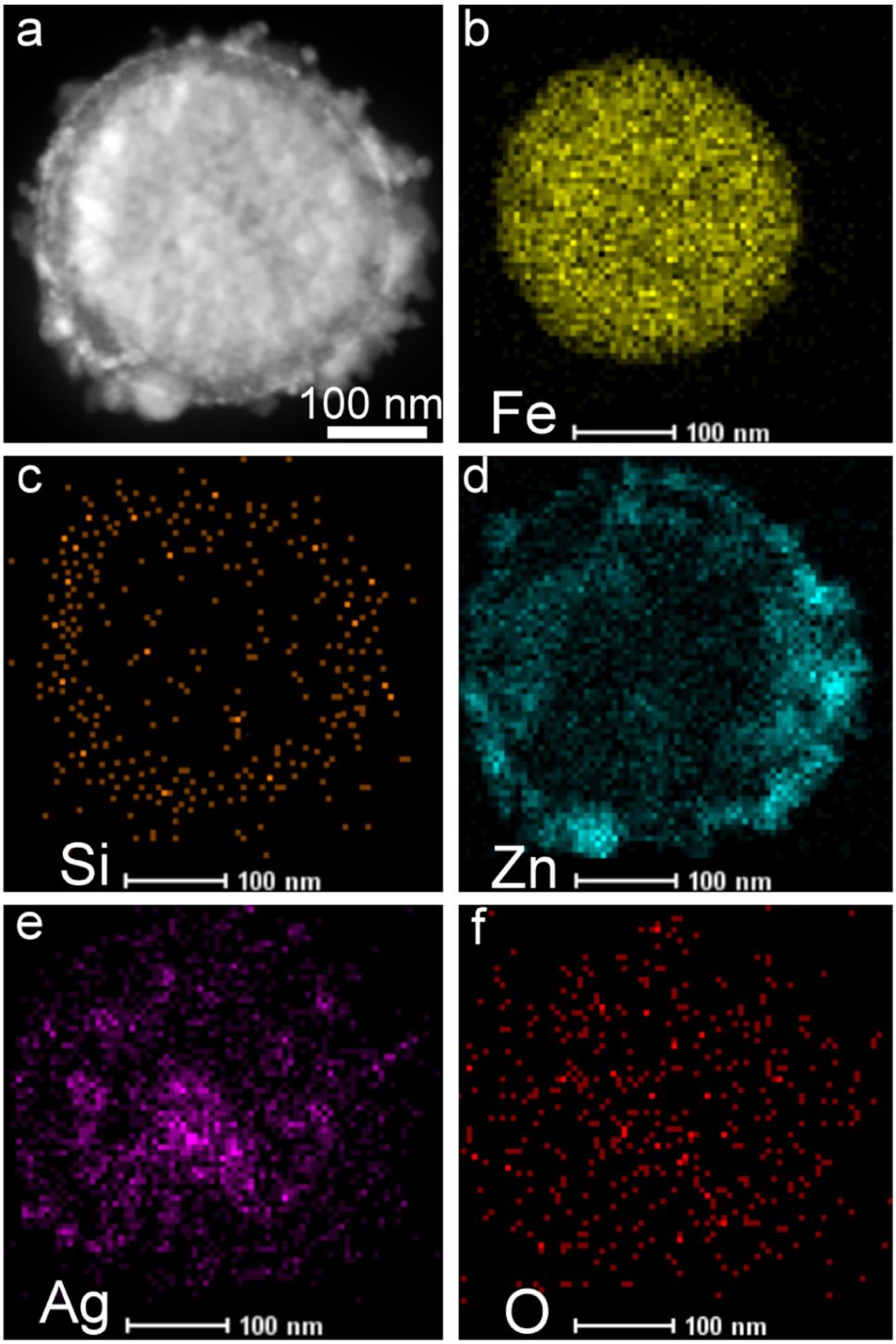

Fig. 3. (a) Typical HAADF image of Fe_3O_4@SiO_2@ZnO–Ag microsphere, (b–f) elemental mapping of a single Fe_3O_4@SiO_2@ZnO–Ag microsphere from the TEM images based on Fe, Si, Zn, Ag and O.

[21]. The change in absorption spectra of the RhB solution over time using Fe_3O_4@SiO_2@ZnO–Ag composites as photocatalysts is shown in Fig. 7a. The typical absorption peak at 553 nm disappeared completely after 90 min, indicating the complete removing of RhB by the Fe_3O_4@SiO_2@ZnO–Ag composite photocatalysts.

The changes in the Photodegradation efficiency versus irradiation time in the presence of Fe_3O_4@SiO_2@ZnO or Fe_3O_4@SiO_2@ZnO–Ag were measured and are shown in Fig. 7b. For comparison, the blank test was carried out under the same condition except that no photocatalyst was added in the photocatalytic reaction system. The result of the blank test demonstrates that the photolysis of RhB is extremely slow. Similarly, no obvious enhancement of degradation efficiency is found for Fe_3O_4@SiO_2, just reaching 11% after 90 min irradiation. As shown in Fig. 7b, Fe_3O_4@SiO_2@ZnO–Ag could eliminate RhB completly under 90 min UV light, while the Fe_3O_4@SiO_2@ZnO could only remove 65.2% RhB under the same condition.

The photocatalytic activity of Fe_3O_4@SiO_2@ZnO core–shell microspheres can be significantly enhanced by loading Ag nanoparticles. The positive effect of Ag deposits is commonly due to the fact

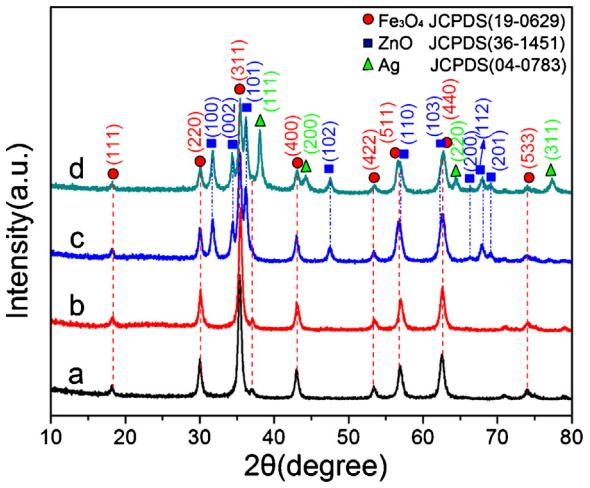

Fig. 4. XRD patterns of (a) Fe_3O_4, (b) Fe_3O_4@SiO_2, (c) Fe_3O_4@SiO_2@ZnO, (c) Fe_3O_4@SiO_2@ZnO–Ag.

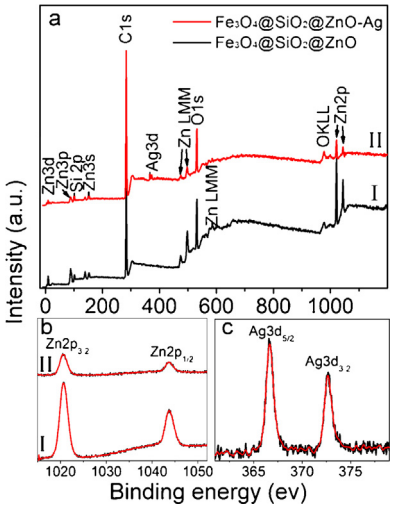

Fig. 5. (a) XPS fully scanned spectra and (b) XPS spectra of Zn2p for (I) Fe_3O_4@SiO_2@ZnO and (II) Fe_3O_4@SiO_2@ZnO–Ag. (c) XPS spectrum of Ag3d for Fe_3O_4@SiO_2@ZnO–Ag.

that Ag nanoparticles on the surface of ZnO act like electron captures, which provide sites for the accumulation of photogenerated electrons, and then enhance the separation of photinduced electron/hole pairs. This can be understood based on the proposed band structure as shown in Fig. 8. As we all known the work function of Ag (4.3 eV) is smaller than that of ZnO (5.2 eV). To make the Fermi

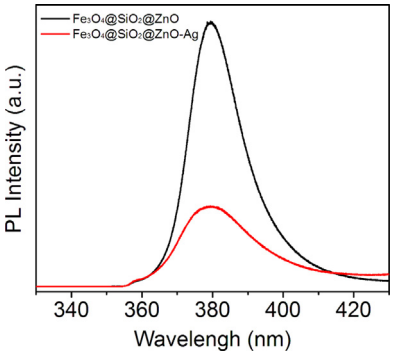

Fig. 6. Photoluminescence (PL) spectra of the prepared Fe_3O_4@SiO_2@ZnO and Fe_3O_4@SiO_2@ZnO–Ag photocatalysts (λ_{ex} = 325 nm)

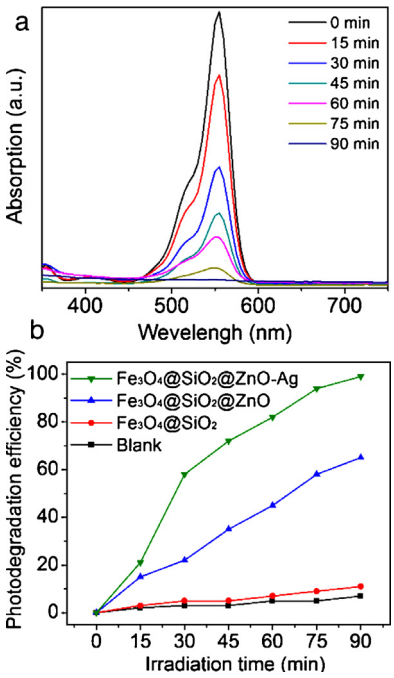

Fig. 7. (a) UV–vis absorption spectra of RhB over time with Fe_3O_4@SiO_2@ZnO–Ag microspheres as photocatalysts and (b) Photodegradation efficiency activity of various types of catalysts.

level equilibration, the electrons should be transfer from Ag to the conduction band (CB) of ZnO. When these core–shell microspheres are irradiated by UV light with photon energy larger or equal to the band gap of ZnO, electrons (e^-) can be excited from VB to the CB and the same amount of holes (h^+) will be generated simultaneous. Subsequently, the electrons accumulated at the CB of ZnO or Ag particles can transferred adsorbed O_2 to produce $^{\bullet}O_2^-$ [40]. Goto et al. have done many efforts on studying O_2 reduction to $^{\bullet}O_2^-$, which accelerate the photocatalytic process [41]. The photoinduced holes are able to react with OH^- to form $^{\bullet}OH$, which is also an important active species to determine the photocatalytic performance of semiconductor photocatalyst [42–44]. It is reported that $^{\bullet}OH$ show little selectivity for degradation of organic contaminants [37].

3.5. Magnetic properties and reusability of samples

Easy separation and reusage are other important advantages for the magnetic core-shell microspheres. The magnetic properties of Fe_3O_4, Fe_3O_4@SiO_2, Fe_3O_4@SiO_2@ZnO, and Fe_3O_4@SiO_2@ZnO–Ag microspheres were investigated here. From the magnetic hystere-

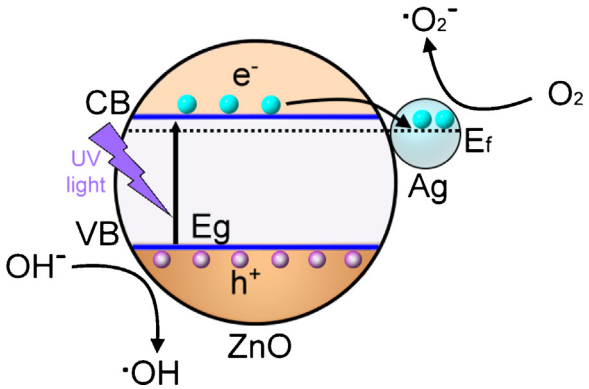

Fig. 8. Schematic energy structure between ZnO and Ag of the Fe_3O_4@SiO_2@ZnO–Ag Composites.

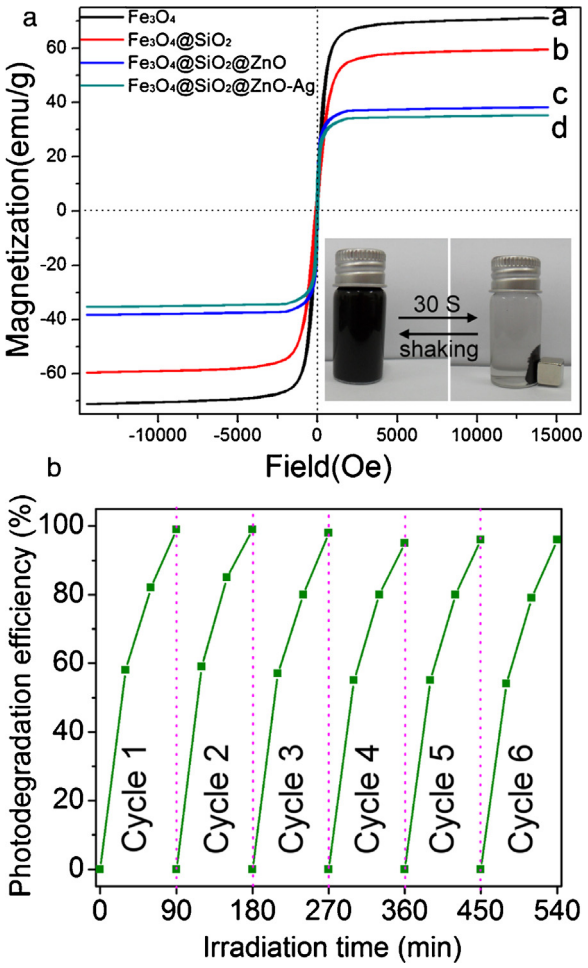

Fig. 9. (a) Magnetic hysteresis loops of the products at room temperature (300 K) (Inset in (a) shows the photograph of a separation and redispersion process of Fe_3O_4@SiO_2@ZnO–Ag microspheres by using a magnet.) (b) The reusability of Fe_3O_4@SiO_2@ZnO–Ag for RhB decoloration.

sis loops of Fig. 9a, it can be concluded that all four products showed superparamagnetic properties, with no obvious remanence or coercivity at 300 K. The magnetization saturation values (Ms) of the Fe_3O_4 microspheres were first measured, and the value reached to 71.1 emu × g^{-1}. Upon coating of a SiO_2 layer, the Ms value for the Fe_3O_4@SiO_2 microspheres was reduced to 59.5 emu × g^{-1}. In addition, after coating ZnO and Ag nanoparticles, their Ms values were further decreased to 38.3 and 35.4 emu × g^{-1}, respectively. However, the final Ms value of Fe_3O_4@SiO_2@ZnO–Ag microspheres was sufficiently high to allow for efficient separation and purification. As shown in the inset photograph in Fig. 9a, with an external magnet, the homogeneous dispersion of the Fe_3O_4@SiO_2@ZnO–Ag microspheres could be separated quickly from the solution and form aggregates in only 30 s. While removing the magnet, the aggregates were redispersed into the solution quickly by a slightly shaking. The superparamagnetic feature is extremely important for photocatalysts. To test the reusability of the core–shell Fe_3O_4@SiO_2@ZnO–Ag microspheres, we repeat the photocatalytic experiments with the same sample for six times, using a magnet to separate the photocatalysts from solution after each test. As shown in Fig. 9b, the sample maintains good photocatalytic activity even after six circles. To study the photo stability of ZnO, XRD patterns of Fe_3O_4@SiO_2@ZnO–Ag before and after RhB discoloration are given in Fig. 10. According to Fig. 10 there was no obviously change between two patterns. This result demonstrated that these core–shell Fe_3O_4@SiO_2@ZnO–Ag microspheres

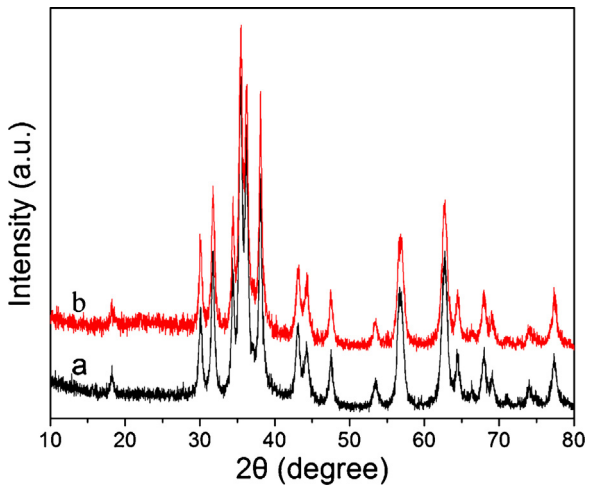

Fig. 10. XRD patterns of Fe_3O_4@SiO_2@ZnO–Ag (a) before and (b) after RhB discoloration.

have an excellent chemical stability and can serve as recyclable photocatalysts for many practical applications.

4. Conclusions

In summary, we successfully synthesized magnetically retrievable Fe_3O_4@SiO_2@ZnO–Ag microspheres with well designed core–shell structure and excellent photocatalytic performance. The unique structural design endows the as-prepared photocatalyst with multiple important characteristics based on the synergetic interaction between different components: it contains a sensitive magnetic core for easy magnetic recycling, an inert SiO_2 interlayer for preventing the Fe_3O_4 shell from photocorrosion or chemical corrosion, and preventing the transfer of electrons–holes between ZnO and core particles from decreasing the photocatalytic activity, and ZnO shell with Ag nanoparticles loaded on the surface for improved photocatalytic efficiency. This core–shell photocatalyst shows excellent efficiency toward the photodegradation of Rhodamine B (RhB) under UV light in aqueous environment as well as high stability and recyclability. Therefore, the easy magnetic recycling, excellent chemical stability, and the enhanced photocatalytic performance, and recovery, and accessible synthetic route make the core–shell Fe_3O_4@SiO_2@ZnO–Ag microspheres have great application prospects in wastewater treatments.

Acknowledgments

This work is supported by the National Programs for High Technology Research and Development of China (863) (Item No. 2013AA032202), National Natural Science Foundation of China (Grant Nos. 61378085, 51479220 and 61308095), Program for the development of Science and Technology of Jilin province (Item No. 20130102004JC, 201215222 and 20140101205JC).

References

[1] D.Q. Zhang, G.S. Li, J.C. Yu, J. Mater. Chem. 20 (2010) 4529–4536.
[2] H. Kyung, J. Lee, W. Choi, Environ. Sci. Technol. 39 (2005) 2376–2382.
[3] C.C. Chen, W.H. Ma, J.C. Zhao, Chem. Soc. Rev. 39 (2010) 4206–4219.
[4] T. Ochiai, A. Fujishima, J. Photochem. Photobiol. C: Photochem. Rev. 13 (2012) 247–262.
[5] A. Fujishima, K. Honda, Nature 238 (1972) 37–38.
[6] J.M. Cai, Y.M. Zhu, D.S. Liu, M. Meng, Z.P. Hu, Z. Jiang, ACS Catal. 5 (2015) 1708–1716.
[7] M.D. Ye, M.Y. Wang, D.J. Zheng, N. Zhang, C.J. Lin, Z.Q. Lin, Nanoscale 6 (2014) 3576–3584.
[8] R.M. Mohamed, E.S. Aazam, Appl. Catal. A: Gen. 480 (2014) 100–107.

[9] S.Y. Hao, J. Hou, P.L. Aprea, T.X. Lv, Ind. Eng. Chem. Res. 53 (2014) 14617–14622.
[10] D.S. Bohle, C.J. Spina, J. Am. Chem. Soc. 131 (2009) 4397–4404.
[11] R. Singh, B. Pal, J. Mol. Catal. A: Chem. 396 (2015) 15–22.
[12] M.R. Hoffmann, S.T. Martin, W. Choi, D.W. Bahnemann, Chem. Rev. 95 (1995) 69–96.
[13] X.J. Bai, L. Wang, R.L. Zong, Y.H. Lv, Y.Q. Sun, Y.F. Zhu, Langmuir 29 (2013) 3097–3105.
[14] N. Pan, H. Xue, M. Yu, X. Cui, X. Wang, J.G. Hou, J. Huang, S.Z. Deng, Nanotechnology 21 (2010) 225707.
[15] J. Lee, H.S. Shim, M. Lee, J.K. Song, D. Lee, J. Phys. Chem. Lett. 2 (2011) 2840–2845.
[16] D.D. Lin, H. Wu, R. Zhang, W. Pan, Chem. Mater. 21 (2009) 3479–3484.
[17] Q.W. Ding, Y.E. Miao, T.X. Liu, ACS Appl. Mater. Interfaces 5 (2013) 5617–5622.
[18] Z.C. Liu, Z.F. Liu, T. Cui, J.W. Li, J. Zhang, T. Chen, X.C. Wang, X.P. Liang, Chem. Eng. J. 235 (2014) 257–263.
[19] A. Haarstrick, O.M. Kut, E. Heinzle, Environ. Sci. Technol. 30 (1996) 817–824.
[20] W. Wu, C.Z. Jiang, V.A.L. Roy, Nanoscale 7 (2015) 38–58.
[21] Z. Liu, F.T. Chen, Y.P. Gao, Y. Liu, P.F. Fang, S.J. Wang, J. Mater. Chem. A 1 (2013) 7027–7030.
[22] C. Karunakaran, P. Vinayagamoorthy, J. Jayabharathi, Langmuir 30 (2014) 1503–15039.
[23] X.F. Bian, K.Q. Hong, X. Ge, R. Song, L.Q. Liu, M.X. Xu, J. Phys. Chem. C 119 (2015) 1700–1705.
[24] T.T. Baby, S. Ramaprabhu, Talanta 80 (2010) 2016–2022.
[25] J.P. Cheng, R. Ma, M. Li, J.S. Wu, F. Liu, X.B. Zhang, Chem. Eng. J. 210 (2012) 80–86.
[26] M.Y. Zhang, L. Li, Y. Liu, L.L. Xu, X.T. Zhang, J. Mol. Catal. A: Chem. 400 (2015) 154–161.
[27] L. Ge, J. Mol. Catal. A: Chem. 282 (2008) 62–66.
[28] L.L. Sun, W. Wu, S.L. Yang, J. Zhou, M.Q. Hong, X.H. Xiao, F. Ren, C.Z. Jiang, ACS Appl. Mater. Interfaces 6 (2014) 1113–1124.
[29] P. Li, Z. Wei, T. Wu, Q. Peng, Y.D. Li, J. Am. Chem. Soc. 133 (2011) 5660–5663.
[30] M. Moonsiri, P. Rangsunvigit, S. Chavadej, E. Gulari, Chem. Eng. J. 97 (2004) 241–248.
[31] S.A. Ansari, M.M. Khan, M.O. Ansari, J. Lee, M.H. Cho, J. Phys. Chem. C 117 (2013) 27023–27030.
[32] L.Q. Jing, D.J. Wang, B.Q. Wang, S.D. Li, B.F. Xin, H.G. Fu, J.Z. Sun, J. Mol. Catal. A: Chem. 244 (2006) 193–200.
[33] H.R. Liu, G.X. Shao, J.F. Zhao, Z.X. Zhang, Y. Zhang, J. Liang, X.G. Liu, H.S. Jia, B.S. Xu, J. Phys. Chem. C 116 (2012) 16182–16190.
[34] H. Deng, X.L. Li, Q. Peng, X. Wang, J.P. Chen, Y.D. Li, Angew. Chem. Int. Ed. 44 (2005) 2782–2785.
[35] W. Stöber, A. Fink, E. Bohn, J. Colloid Interface Sci. 26 (1968) 62–69.
[36] Y. Chi, Q. Yuan, Y.J. Li, L. Zhao, N. Li, X.T. Li, W.F. Yan, J. Hazard. Mater. 262 (2013) 404–411.
[37] W.W. Lu, S.Y. Gao, J.J. Wang, J. Phys. Chem. C 112 (2008) 16792–16800.
[38] Q. Deng, X. Duan, H.L. Dickon, H. Tang, Y. Yang, M. Kong, ACS Appl. Mater. Interfaces 4 (2012) 6030–6037.
[39] M.M. Khan, S.A. Ansari, J.A. Lee, M.H. Cho, Nanoscale 5 (2013) 4427–4435.
[40] J.G. Yu, J.F. Xiong, B. Cheng, S.W. Liu, Appl. Catal. B: Environ. 60 (2005) 211–221.
[41] H. Goto, Y. Hanada, T. Ohno, M. Matsumura, J. Catal. 225 (2004) 223–229.
[42] L.Y. Zhang, L.W. Yin, C.X. Wang, N. Lun, Y.X. Qi, ACS Appl. Mater. Interfaces 2 (2010) 1769–1773.
[43] D.M. Chen, Z.H. Wang, T.Z. Ren, H. Ding, W.Q. Yao, R.L. Zong, Y.F. Zhu, J. Phys. Chem. C 118 (2014) 15300–15307.
[44] S. Khanchandani, P.K. Srivastava, S. Kumar, S. Ghosh, A.K. Ganguli, Inorg. Chem. 53 (2014) 8902–8912.